

Influence of the Nd 4*f* states on the magnetic behavior and the electric field gradient of the oxypnictides superconductors NdFeAsO_{1-x}F_x

P. Jeglič,¹ J.-W. G. Bos,^{2,*} A. Zorko,¹ M. Brunelli,³ K. Koch,⁴ H. Rosner,⁴ S. Margadonna,^{2,†} and D. Arčon^{1,5,‡}

¹*Institute "Jozef Stefan", Jamova 39, 1000 Ljubljana, Slovenia*

²*School of Chemistry, University of Edinburgh, West Mains Road, EH9 3JJ, United Kingdom*

³*European Synchrotron Radiation Facility, BP 220, 38043 Grenoble Cedex, France*

⁴*Max-Planck Institute for Chemical Physics of Solids, Nöthnitzer Str. 40, 01187 Dresden, Germany*

⁵*Faculty of Mathematics and Physics, University of Ljubljana, Jadranska 19, 1000 Ljubljana, Slovenia*

The structural, electronic, and magnetic properties of the superconducting NdFeAsO_{1-x}F_x phases ($T_C = 43$ K for $x = 0.15$) have been investigated experimentally by high-resolution synchrotron x-ray powder diffraction, magnetization and ⁷⁵As NMR measurements. Density-functional calculations were performed to calculate and analyze the electric field gradient and the density of states. Compared to LaFeAsO family, the NdFeAsO family shows a contraction of the lattice parameters with shorter rare-earth (RE)-As bond distances, an increased thickness of the As-Fe₂-As layer, and less distorted Fe-As₄ tetrahedra. The ⁷⁵As quadrupole frequencies are enhanced with respect to the La analogs. This is due to a more prolate As 4*p* electron distribution mainly caused by the reduced lattice parameters and not by the presence of Nd 4*f* electrons. A non-negligible hyperfine coupling between the ⁷⁵As nuclei and the Nd 4*f* states indicates a weak coupling between the REO and FeAs layer and possibly opens the channel for a Ruderman-Kittel-Kasuya-Yosida (RKKY)-type interaction between localized Nd 4*f* moments mediated by itinerant Fe 3*d* and/or Nd 5*d* states.

PACS numbers: 74.70.-b, 76.60.-k

I. INTRODUCTION

The family of rare-earth (RE) quaternary oxypnictides with the general formula REFeAsO (RE = La, Ce, Pr, Nd, Sm, Gd, Tb, Dy) (Ref. 1) is currently generating much excitement in the condensed matter community. When electron doped (e.g., partial replacement of O²⁻ with F⁻ or oxygen deficiency), these materials are reported to display superconductivity with a superconducting transition temperature, T_C , as high as 55 K.^{2,3,4,5,6,7,8,9,10} In electron-doped LaFeAsO the superconductivity ($T_C \sim 26$ K) appears in the close vicinity to a spin-density wave ground state,^{8,11,12} implying that antiferromagnetic (AF) correlations may be important in the promotion of the superconducting ground state. La³⁺ has no unpaired electrons, and the magnetic response can be attributed solely to the Fe 3*d* electronic states that dominate the region around the Fermi level. The relation between AF fluctuations and superconductivity has been proposed theoretically^{13,14} and addressed experimentally by ¹⁹F, ⁷⁵As, and ¹³⁹La NMR^{15,16,17}. Upon F doping, a pseudo-gap behavior has been found in the temperature dependence of the ¹⁹F (Ref. 15) and ⁷⁵As (Ref. 17) spin-lattice relaxation rates.

Substitution of La³⁺ with other rare-earth elements such as Nd³⁺ (free-ion magnetic moment $\mu \sim 3.6 \mu_B$) introduces additional spin degrees of freedom in the REO layer due to the unpaired RE 4*f* electrons. Interestingly, the NdFeAsO_{1-x}F_x family displays superconductivity with enhanced T_C 's of ~ 50 K compared to the La-based materials.^{2,7} This raises important questions of if and how the rare-earth magnetic moment interacts with the conducting FeAs layer and whether these 4*f* moments or lattice effects (chemical pressure) have a stronger influ-

ence on the electronic structure and the related magnetic and superconducting properties in the REFeAsO family.

To address these questions, we have studied the structural, magnetic, and superconducting properties of the NdFeAsO_{1-x}F_x family by means of high-resolution synchrotron x-ray powder diffraction, magnetization, and ⁷⁵As NMR measurements. Our experimental results are supported by electronic structure calculations.

II. METHODS

Polycrystalline NdFeAsO and NdFeAsO_{0.85}F_{0.15} samples were prepared by a standard two-step solid-state reaction method. The magnetic susceptibility was measured using a Quantum Design magnetic property measurement system. Synchrotron powder diffraction data sets, collected on the ID31 high-resolution diffractometer at the European Synchrotron Radiation Facility in Grenoble, France, were binned with a 0.002° stepsize ($\lambda = 0.309952$ Å). The GSAS suite of programs and EXPGUI graphical user interface were used for Rietveld fitting.^{18,19} ⁷⁵As ($I = 3/2$) NMR frequency-swept spectra were measured in 8.9 T magnetic field with a selective solid echo pulse sequence (pulse length of $\pi/2 = 22 \mu s$ and delay of $\tau = 50 \mu s$). The reference frequency of $\nu(^{75}\text{As}) = 65.096$ MHz was determined from a NaAsF₆ standard.

The band-structure calculations were performed using the full-potential local-orbital minimum basis code FPLO (version 5.00-19) (Ref. 20) within the local density approximation(LDA). In the scalar relativistic calculations the exchange and correlation potential of Perdew and Wang²¹ was employed. To treat the Nd 4*f* state

adequately LSDA+ U in the atomic limit was employed with $U^{\text{Nd}} = [7, 9]$ eV and $J = 0.7$ eV. As basis set Nd (4p4d4f5s5p/6s6p5d+7s7p), Fe (3s3p/4s4p3d+5s5p), As (3p/4s4p3d+5s5p) and O (2s2p3d+3s3p) were chosen for semicore/valence+polarization states. The high lying states improve the basis which is especially important for the calculation of the electric field gradient (EFG) tensor with components $V_{ij} = \partial V / \partial x_i \partial x_j$. The lower lying states were treated fully relativistic as core states. A well converged k mesh of 252 k points was used in the irreducible part of the Brillouin zone. In order to investigate the influence of F substitution on the O site, the virtual crystal approximation (VCA) was applied.

III. RESULTS

High-resolution synchrotron x-ray powder diffraction profiles of NdFeAsO at room temperature confirmed that its structure is tetragonal—space group $P4/nmm$ —in analogy to other REFeAsO systems. Rietveld analysis of the synchrotron X-ray powder diffraction data (Fig. 1) resulted in lattice parameters $a = 3.96629(1)$ Å and $c = 8.59886(6)$ Å with Fe-As and Fe-Fe distances of 2.4007(4) Å and 2.80459(1) Å, respectively and an As-Fe-As bond angle of $111.39(3)^\circ$ [$\chi^2 = 2.4$, $wRp = 13.2\%$, $Rp = 9.2\%$, Nd: $z = 0.13887(6)$, and As: $z = 0.65735(9)$].²² Compared to LaFeAsO,¹¹ the Nd³⁺ containing oxypnictide shows a contraction of the lattice constants with shorter RE-As bond distances, an increased thickness of the As-Fe₂-As layer and less distorted Fe-As₄ tetrahedra. Temperature-dependent synchrotron x-ray powder diffraction measurements collected between room temperature and 100 K revealed the presence of a structural phase transition to an orthorhombic (O) superstructure ($a_O \sim b_O = \sqrt{2}a_T$ and $c_O = c_T$; space group $Cmma$) in analogy with the results reported in Ref. 23. All the Bragg reflections containing the tetragonal Miller indexes $h \neq 0$ and $k \neq 0$ start broadening at 160 K and finally split only at 140 K (inset to Fig. 1).

The F-doped compound, with nominal composition NdFeAsO_{0.85}F_{0.15}, also adopts tetragonal symmetry but with reduced room temperature lattice parameters [$a = 3.96251(1)$ Å and $c = 8.57785(6)$ Å] and Fe-As and Fe-Fe distances of 2.4025(6) Å and 2.80192(1) Å, respectively ($\chi^2 = 2.4$, $wRp = 12.84\%$, $Rp = 10.31\%$, Nd: $z = 0.14211(6)$, and As: $z = 0.6544(1)$). We notice that despite the smaller ionic radius of F[−] compared to O^{2−}, the RE-O distance increases, resulting in an increased thickness of the Nd-O₂-Nd layer and more regular Nd₄-O tetrahedra.

The zero-field-cooled (ZFC) molar magnetic susceptibility, χ , of NdFeAsO measured in a 10 kOe applied field shows a substantial Curie-Weiss-type contribution [Fig. 2a] that completely dominates χ at low temperatures. Analysis of the susceptibility data gives the Curie constant $C = 1.43(2)$ emuK/mol and the Curie-Weiss temperature $\theta = -14(1)$ K [inset to Fig. 2a]. The Curie

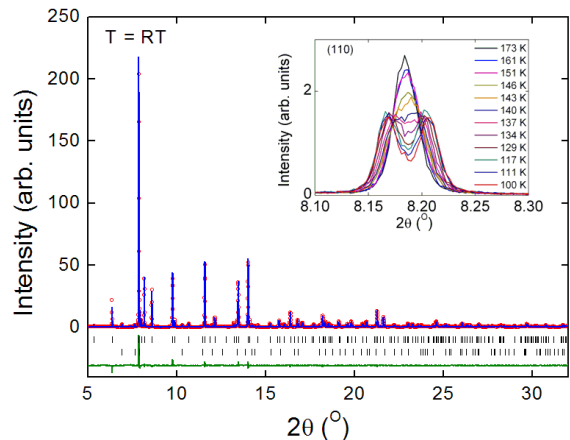


FIG. 1: (Color online) Measured (\circ) and calculated ($-$) synchrotron x-ray powder diffraction ($\lambda = 0.309952$ Å, room temperature) profiles for NdFeAsO. The lower solid line shows the difference profile, and the tick marks show the reflection positions (top: NdFeAsO, bottom: Nd₂O₃ impurity). The inset illustrates the T - O structural phase transition.

constant corresponds to an effective magnetic moment $\mu_{eff} = 3.31(4) \mu_B$ in agreement with the expected value for localized Nd 4f moments, while the negative Curie-Weiss temperature implies AF interactions between the Nd 4f moments. We also note here that the concentration of Nd₂O₃ impurities is so small that the values of C and θ do not change after molar susceptibility is corrected for the impurity contribution. The temperature dependence of the zero-field-cooled magnetization measured on NdFeAsO_{0.85}F_{0.15} [Fig. 2b] shows a clear onset of bulk superconductivity at $T_C = 43(1)$ K with shielding fraction of 40%.

Representative powder ⁷⁵As NMR spectra of NdFeAsO and NdFeAsO_{0.85}F_{0.15} are shown in Fig. 3. The room-temperature spectra for both samples display a typical quadrupole powder line shape. For undoped NdFeAsO the shape of the central $-1/2 \leftrightarrow 1/2$ transition and the sharp singularities for the satellite transitions strongly indicate that the asymmetry parameter, defined by the components of the EFG tensor as $\eta = (V_{xx} - V_{yy}) / V_{zz}$, is $\eta = 0$. V_{zz} defines the quadrupole frequency

$$\nu_Q = \frac{3}{2} \frac{eV_{zz}Q}{I(2I-1)}, \quad (1)$$

with Q as the quadrupole moment of ⁷⁵As. We recall that the ⁷⁵As nuclei have four nearest-neighbor Fe atoms (inset to Fig. 3) and in the tetragonal phase reside on the 2c ($1/4, 1/4, z$) position, which is fourfold axially symmetric. $\eta = 0$ is therefore fully consistent with the As site symmetry. The ⁷⁵As powder NMR line shape simulation (inset to Fig. 5) then gives $\nu_Q = 11.8(1)$ MHz. We note that ν_Q is significantly enhanced compared to $\nu_Q = 8.7(4)$ MHz

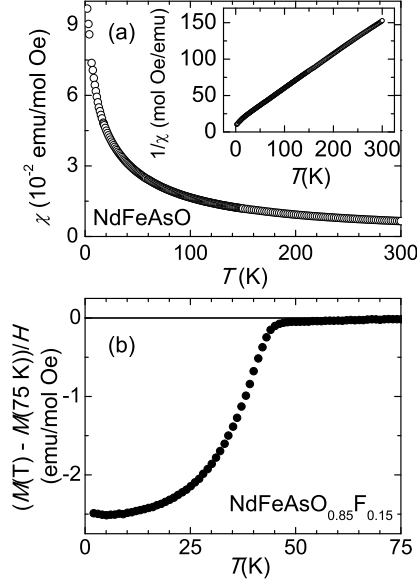


FIG. 2: (a) Temperature dependence of the ZFC susceptibility measured in 10 kOe applied field for NdFeAsO powder. Inset: temperature dependence of the inverse ZFC susceptibility for NdFeAsO powder. (b) Temperature dependence of the ZFC magnetization for NdFeAsO_{0.85}F_{0.15} with the superconducting transition temperature of 43 K and a shielding fraction of 40.6%. The magnetic field was set to 20 Oe.

(Ref. 24) for LaFeAsO and it is even larger than $\nu_Q = 11.00(5)$ MHz reported for LaFeAsO_{0.9}F_{0.1}.¹⁷ This is presumably a result of slightly different charge distributions around the As site reflecting the small structural variations in the As local environment as it will be discussed below. The ⁷⁵As NMR spectra of NdFeAsO_{0.85}F_{0.15} are considerably broader compared to the parent compound, reflecting local disorder introduced by the F doping. This prevents a precise determination of η . However, the ⁷⁵As NMR spectra can be simulated using a Gaussian distribution of ν_Q with a mean value of $\nu_Q = 12.9(2)$ MHz and a full width at half height of the Gaussian distribution $\Delta\nu_Q = 1.8(2)$ MHz.

For the undoped compound, the measured EFG is obtained by applying the ⁷⁵As quadrupole moment²⁵ $Q = (0.314 \pm 0.006)$ b in Eq. (1) and yields $|V_{zz}^{exp}| = (3.11 \pm 0.09) \cdot 10^{21}$ V/m². Using the experimental room temperature lattice parameters and atomic positions and $U^{Nd} = 8$ eV we obtain a good agreement for the calculated EFG: $V_{zz}^{calc} = -3.39 \cdot 10^{21}$ V/m². Varying U^{Nd} by ± 1 eV (within the physically reasonable range) changes the EFG only by $\mp 0.01 \cdot 10^{21}$ V/m², which is well below the experimental error bars. Like for the Fe magnetic moment, which in the calculations shows a strong dependence on the As z position,^{26,27} we observe also for the EFG a strong As z dependence (inset to Fig. 4). The calculated EFG ($V_{zz}^{calc} = -2.92 \cdot 10^{21}$ V/m²) is even closer to the measured one when As is shifted along the neg-

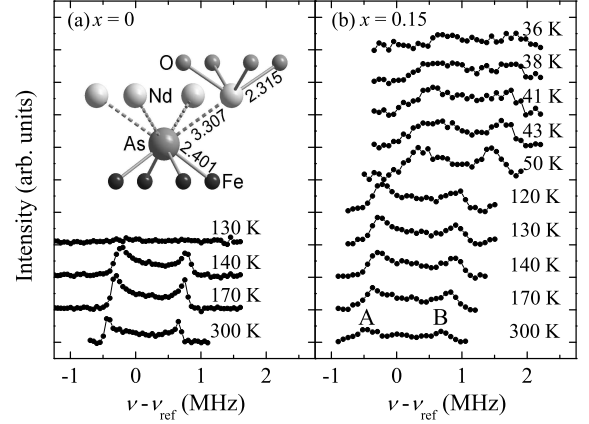


FIG. 3: Representative ⁷⁵As NMR spectra measured in (a) the parent NdFeAsO and (b) the F-doped NdFeAsO_{0.85}F_{0.15} powder samples. Inset: structure around the As ion showing its room-temperature distances to nearest-neighbor Fe (black spheres) and Nd ions (white spheres).

ative z direction to $z = 0.6515$. Here, the energy has a minimum (in inset to Fig. 4 marked by an arrow) and the structure has a shorter Fe-As distance of 2.3729 Å.

Analogous to the experiments, where the quadrupole frequency for ⁷⁵As is larger for the Nd than for the La compound, the magnitude of the calculated $|V_{zz}|$ is larger for the Nd compound $V_{zz} = -3.39 \cdot 10^{21}$ V/m² than for the La compound²⁸ $V_{zz} = -3.21 \cdot 10^{21}$ V/m² but less drastically. Analysis of the calculated EFG (Ref. 29) shows that the largest contribution to the EFG mainly originates from As 4*p* electrons. In both compounds the anisotropy count $\Delta_p = \frac{1}{2}(n_x + n_y) - n_z$ for the As 4*p* electrons is negative, which corresponds to a prolate *p* electron distribution and is in agreement with the negative V_{zz} . For the La compound Δ_p is less negative than for the Nd compound: $\Delta_p = -0.018$ and $\Delta_p = -0.062$, respectively, which means that the 4*p* orbitals are less isotropic for the Nd compound and hence the EFG is enhanced. The observed difference between the La and Nd compounds could arise from either the additional 4*f* electrons due to screening effects or from the smaller lattice parameters in the Nd compound. To separate the influence of the change in the lattice geometry from the change in the electronic configuration, we compare the real EFGs with fictitious EFGs, which are obtained by exchanging the lattice parameters for both compounds (see Table I).

The $|V_{zz}|$ value increases with lattice compression both for the LaFeAsO and NdFeAsO electronic configurations (Table I from the left to the right). Next, we checked the role of the RE 4*f* electrons. In this case we find the opposite trend; i.e., for given lattice parameters $|V_{zz}|$ is smaller for the Nd than for the La compound (Table I from top to bottom). One can therefore conclude that $|V_{zz}|$ increases with lattice contraction and decreases with increasing number of RE 4*f* electrons.

TABLE I: Calculated V_{zz} for As for both compounds for both lattice parameters. In the calculations we used the following room-temperature lattice parameters: set 1 [LaFeAsO (Ref. 11)]: $a=4.03007(9)$ Å, $c=8.7368(2)$ Å, As: $z = 0.6507(4)$, and La: $z = 0.1418(3)$; set 2 (NdFeAsO, this work): $a = 3.96629(1)$ Å and $c = 8.59886(6)$ Å; As: $z = 0.65735(9)$ and Nd: $z = 0.13887(6)$. LaFeAsO with set 1 and NdFeAsO with set 2 are the real compounds; the other combinations are fictitious.

| | Set 1 | Set 2 |
|---------|--|--|
| LaFeAsO | $-3.21 \cdot 10^{21}$ V/m ² | $-3.60 \cdot 10^{21}$ V/m ² |
| NdFeAsO | $-2.92 \cdot 10^{21}$ V/m ² | $-3.39 \cdot 10^{21}$ V/m ² |

Now, we focus on the effect of electron doping on the EFG in NdFeAsO. The EFGs of the doped compounds were calculated with the virtual crystal approximation. The validity of the VCA was confirmed by supercell calculations.³⁰ First, we consider solely the effect of electron doping. Therefore, we keep the structural parameters fixed for different levels of doping. In Fig. 4 two such VCA curves are shown. When the experimentally determined As $z = 0.65735(9)$ position (NdFeAsO at room temperature) is used, the calculated and measured EFG values for 15% doping agree very well. The VCA curve with the optimized As $z = 0.6515$ position deviates from the experimental curve as it systematically predicts a smaller $|V_{zz}|$. Next, we investigate the structural change on top of the doping by calculating the EFG within VCA for the room-temperature structural parameters of NdFeAsO_{0.85}F_{0.15}. We notice that the use of these parameters slightly reduces $|V_{zz}|$ to $V_{zz} = -3.17 \cdot 10^{21}$ V/m². Please note the black circle marked by an arrow in Fig. 4. We stress at this point, that the effect of electron doping on the EFG is much smaller than the influence of the As z position as can be clearly seen by comparing Fig. 4 with the inset of Fig. 4. Our calculations predict a small decrease in $|V_{zz}|$ upon electron doping for NdFeAsO_{0.85}F_{0.15}, although experimentally a slight increase is observed. This is also the case for the La compound where the difference between the slopes of the calculated and the experimental EFGs upon doping²⁸ is even more pronounced. Further studies are required to investigate if this is due to the quality of the samples or due to intrinsic changes in the electronic structure.

In undoped NdFeAsO the ⁷⁵As NMR line shape starts to change below $T_S \sim 160$ K (Fig. 3). Its evolution can be accounted for by assuming that η suddenly starts to increase below T_S and reaches $\eta = 0.10(2)$ at 140 K. The increase in η is a strong indication that the ⁷⁵As site symmetry has lowered due to the structural phase transition to a low-temperature orthorhombic structure (space group $Cmma$),²³ similarly as found in other RE-OfAs systems. We note that in the orthorhombic phase ⁷⁵As is on the $4g$ $(0, 1/4, z)$ position, allowing η to differ from zero. The band-structure calculations show that the influence of the orthorhombic distortion on the EFG is

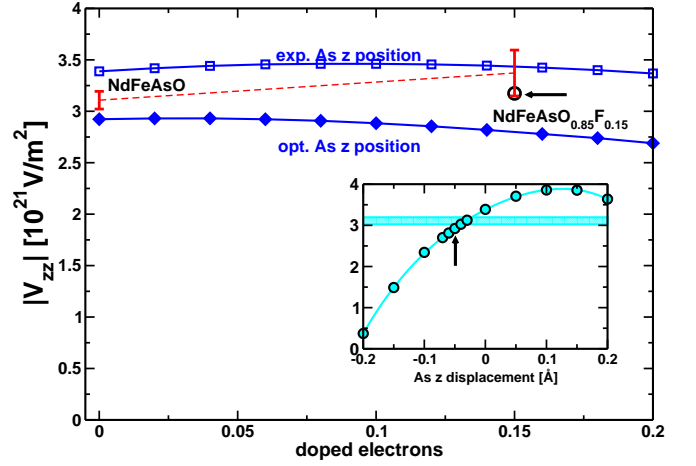


FIG. 4: (Color online) Calculated V_{zz} obtained from the virtual crystal approximation using the experimental As $z = 0.65735(9)$ position (empty squares), the optimized As $z = 0.6515$ (filled diamonds) position, and the NdFeAsO_{0.85}F_{0.15} structure at room temperature (black circle marked by an arrow). The measured EFGs for the pure and the 15% F-doped compound are shown by error bars. Inset: dependence of ⁷⁵As V_{zz} on the As z position. The optimized As z position is marked by an arrow. The experimental V_{zz} is represented by the shaded bar.

negligible – much less than the experimental error bars. This is understandable given the small size of the orthorhombic splitting. The anisotropy parameter is more sensitive to the distortion and increases to $\eta = 0.04$ (compare to the experimental value of $\eta = 0.10(2)$). Below $T_N = 140$ K the high-temperature ⁷⁵As resonance in NdFeAsO starts to rapidly lose in intensity on the account of an extremely broad low-temperature signal (inset to Fig. 5). The dramatic broadening of the ⁷⁵As resonance is a manifestation of AF magnetic order of Fe moments occurring at $T_N = 140$ K, which was previously observed by μ SR (Ref. 31) and neutron-diffraction³² measurements. In the doped NdFeAsO_{0.85}F_{0.15} both the structural and AF transitions are absent at least down to the superconducting transition temperature $T_C = 43$ K, below which the ⁷⁵As resonance rapidly disappears (Fig. 3). Line-shape simulations also show that ν_Q is almost temperature independent and therefore cannot account for the large temperature dependence of the observed ⁷⁵As NMR shift.

IV. DISCUSSION

In order to understand the observed ⁷⁵As resonance for the undoped NdFeAsO in the AF phase, we assume that this phase is characterized by the spin-density wave vector $\vec{Q} = (1, 0, 1)$ and that the ordered Fe magnetic moments are aligned along the a axis, i.e., similarly as in LaFeAsO.⁸ μ SR measurements suggested that the Fe ordered moment in NdFeAsO is similar to that of LaFeAsO,

i.e., $\mu_{\text{Fe}} \sim 0.3 \mu_B$.³¹ The shift of the ^{75}As resonance in the AF phase is due to the internal field B_{int} aligned along the crystal c axis and is given by the anisotropic (off-diagonal) part of the hyperfine interaction with Fe moments, a_{xz} , as $B_{\text{int}} = 4a_{xz} \mu_{\text{Fe}}$.³³ Its isotropic part in the ordered phase is filtered out from the shift due to the highly symmetrical position of ^{75}As with respect to Fe moments. The projection of this field adds to the external magnetic field, corrected for an isotropic hyperfine shift caused by Nd moments, B_0 and gives rise to the effective magnetic field $B_{\text{eff}} = B_0 + B_{\text{int}} \cos \vartheta$. Here, ϑ denotes the angle between the external and internal magnetic fields. Taking into account also the first-, $\Delta\nu_Q^{(1)}(\vartheta, \phi)$, and the second-order, $\Delta\nu_Q^{(2)}(\vartheta, \phi)$, quadrupole effects, the ^{75}As resonance frequency reads as

$$\nu_{m \leftrightarrow m-1} = \gamma_{\text{As}} B_{\text{eff}} + \Delta\nu_Q^{(1)}(\vartheta, \phi) + \Delta\nu_Q^{(2)}(\vartheta, \phi). \quad (2)$$

Here, γ_{As} is the ^{75}As gyromagnetic ratio and ϑ and ϕ define the orientation of B_{eff} with respect to the principal axes of EFG tensor. Our simulation with Eq. (1) results in a good fit of the 80 K spectrum when $a_{xz} = 10.5 \text{ kOe}/\mu_B$ was used (inset to Fig. 5). We stress at this point that the large anisotropic hyperfine fields cannot be explained by dipolar fields of the Fe moments and that they rather provide experimental evidence for the Fe 3d and As 4p hybridizations.^{33,34}

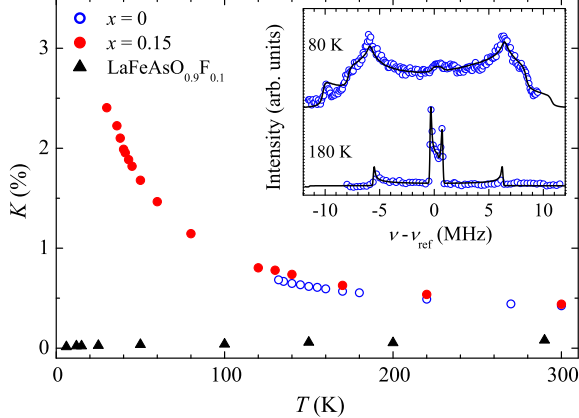


FIG. 5: (Color online) Temperature dependence of the ^{75}As NMR shift measured for undoped NdFeAsO (open circles) and F-doped NdFeAsO_{0.85}F_{0.15} powder samples (solid circles). For comparison we show the corresponding shift measured in LaFeAsO_{0.9}F_{0.1} (solid triangles) (Ref. 17). Inset: the ^{75}As NMR line shape simulations [Eq. 1] for NdFeAsO sample above ($T = 180 \text{ K}$) and below ($T = 80 \text{ K}$) the AF ordering transition $T_N = 140 \text{ K}$.

We now turn to the determination of the isotropic part of the ^{75}As hyperfine interaction measured by the Knight shift, K , in the paramagnetic phase (Fig. 5). We stress that the measured shift is by an order of magnitude larger and has a completely different temperature dependence

when compared to the one for LaFeAsO_{0.9}F_{0.1}.¹⁷ Temperature dependence of K in NdFeAsO_{1-x}F_x can be well described by the Curie-Weiss-type behavior, $K(T) = K_0 + \kappa/(T - \theta)$. The value of the Curie-Weiss temperature $\theta = -13(2) \text{ K}$ [$\kappa = 0.99(2) \text{ K}$] is the same as determined from the magnetic susceptibility. We can therefore assume that the Curie-Weiss part of the shift comes from the Fermi contact hyperfine interaction between the ^{75}As nuclei and Nd 4f moments. The value of $K_0 = 0.096(15)\%$ is close to the total NMR shift reported for LaFeAsO_{0.9}F_{0.1}.¹⁷ We thus associate this part of the ^{75}As NMR shift to the coupling of ^{75}As with the itinerant Fe 3d electrons in the FeAs layer. Interestingly, for undoped NdFeAsO we find that K_0 is slightly reduced, i.e., $K_0 = 0.091(20)\%$.

We proceed with the above analysis by recognizing that K_0 is given by the hyperfine coupling to itinerant FeAs electrons and the orbital part,

$$K_0 = \frac{a_{\text{FeAs}}^{\text{iso}}}{N_A \mu_B} \chi_{\text{FeAs}} + K_{\text{orb}}. \quad (3)$$

Here $K_{\text{orb}} = -0.075\%$ is the orbital shift,¹⁷ N_A and μ_B are the Avogadro number and Bohr magneton, χ_{FeAs} is the molar susceptibility for the itinerant FeAs electrons, and finally $a_{\text{FeAs}}^{\text{iso}}$ is the corresponding isotropic hyperfine coupling constant. Since a precise dependence of χ_{FeAs} is in NdFeAsO_{1-x}F_x completely masked by the magnetism of the Nd 4f moments (Fig. 2), we approximate it with the dependence for LaFeAsO taken from Ref. 17. Using the value of K_0 we derive $a_{\text{FeAs}}^{\text{iso}} = 27.7 \text{ kOe}/\mu_B$ and $a_{\text{FeAs}}^{\text{iso}} = 29 \text{ kOe}/\mu_B$ for NdFeAsO and NdFeAsO_{0.85}F_{0.15}, respectively. Although these values have to be taken with certain caution due to approximations used, we notice that they are about 10%-15% larger than in LaFeAsO_{0.9}F_{0.1}.¹⁷

The contribution arising from the coupling to Nd 4f moments, K_{Nd} , can be expressed as

$$K_{\text{Nd}} = \kappa/(T - \theta) = \frac{a_{\text{Nd}}^{\text{iso}}}{N_A \mu_B} \chi_{\text{Nd}}, \quad (4)$$

where $\chi_{\text{Nd}} = C/(T - \theta)$ is the molar susceptibility of localized Nd 4f moments and $a_{\text{Nd}}^{\text{iso}}$ is the corresponding isotropic hyperfine coupling constant. Using the value of κ we calculate $a_{\text{Nd}}^{\text{iso}} = 3.8 \text{ kOe}/\mu_B$. Although $a_{\text{Nd}}^{\text{iso}}$ is by an order of magnitude smaller than $a_{\text{FeAs}}^{\text{iso}}$, it is still surprisingly large as the REFeAsO system has so far been believed to comprise well isolated Fe-As and REO layers.³⁴

The coexistence of itinerant Fe 3d and localized Nd 4f moments in NdFeAsO_{1-x}F_x is highly intriguing, and one wonders how the magnetic and/or superconducting properties are affected. Our experimental results clearly prove that the ^{75}As NMR probe interacts both with the Fe 3d conducting electrons in the FeAs layer as well as with the localized Nd 4f moments in the NdO layer. The sizeable anisotropic hyperfine coupling constant between ^{75}As and Fe 3d moments ($a_{xz} = 10.5 \text{ kOe}/\mu_B$) in the AF phase has its origin in the hybridization between the Fe 3d and the As 4p states.

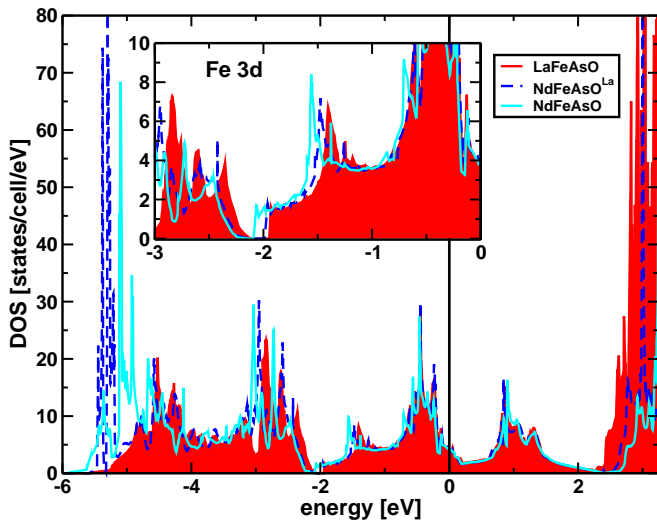


FIG. 6: (Color online) Total density of states for LaFeAsO (shaded red) and NdFeAsO (full light blue line) using the experimental room-temperature structural data. The density of states of the fictitious NdFeAsO (labeled NdFeAsO^{La}, using set 1 in Table I) is shown by the dashed dark blue line. Inset: the density of states of the Fe 3d states for the same three structures.

This result also nicely corroborates with the band-structure calculations and the density of states (DOS). In Fig. 6 the total DOS for LaFeAsO and NdFeAsO (using the room-temperature experimental structural parameters) and the fictitious Nd compound (labeled NdFeAsO^{La} and calculated by using the experimental structure of the La compound at room temperature) is shown. The main features of the total DOS are very similar for the La and the fictitious Nd^{La} compounds—except for the occupied Nd 4f band (around -5 eV). Shorter lattice parameters in the Nd compound (going from the dashed to the full line in Fig. 6) have mainly an effect on the position of the 4f and the Fe 3d states (see below). Like in the La compound, we find also in the Nd compound a strong hybridization of Fe 3d with As 4p states in the energy region between -4 and -2 eV. The differences in these DOS can be seen more clearly on a smaller scale. The Fe 3d states are slightly shifted in direction of lower energy from the La via the fictitious Nd^{La} to the Nd compound; see inset of Fig. 6. These subtle electronic structure changes are also observed in the ⁷⁵As NMR experiment. We notice that the As-Fe isotropic hyperfine coupling constant $a_{\text{FeAs}}^{\text{iso}} = 27.7$ to 29 kOe/ μ_B is about 10% larger than that reported for the La-family. This constant depends on the degree of polarization of the As 4s electrons caused by the As 4p states via exchange polarization effect.³⁵ Therefore it may be—similar to the DOS—sensitive to the small crystalline structure variations such as lattice contraction or the shift of the As along the *z* axis found for NdFeAsO_{1-x}F_x in our x-ray diffraction (XRD) experiments. We conclude that all ⁷⁵As NMR parameters,

a_{xz} , $a_{\text{FeAs}}^{\text{iso}}$ and ν_Q are very sensitive to the details of As 4p electron distribution. Related to that, we refer here to the work of Mukuda et al.²⁴ where the monotonic increase in the superconducting transition temperature T_C with ⁷⁵As quadrupole frequency ν_Q has been reported. Based on these observations, our calculations (Table I) may suggest that it is the lattice contraction and not the presence of additional RE 4f states that shifts T_C to higher values in NdFeAsO_{1-x}F_x compounds. This is also in line with pressure experiments on LaFeAsO, where T_c was increased up to 43 K.³

Finally we comment on the non-negligible coupling between ⁷⁵As and Nd 4f moments, $a_{\text{Nd}}^{\text{iso}} = 3.8$ kOe/ μ_B , which directly evidence an interaction between the REO and FeAs layers. Such interlayer coupling could open the possibility for an indirect exchange interaction between the localized Nd 4f moments mediated by the Fe 3d and/or Nd 5d (partially occupied in the band-structure calculations) conducting electrons, i.e., a Ruderman-Kittel-Kasuya-Yosida (RKKY)-type interaction. The small Curie-Weiss temperature ($\theta = -14$ K) as well as the low ordering temperature for the Nd moments may be due to the long-range nature of the RKKY-type interaction and its oscillatory dependence on the distance between the Nd moments. Additional experiments are needed to shed more light on the size of Nd ordered moment at low temperatures.

V. SUMMARY

In summary, we have performed a study of the structural, electronic and magnetic properties of the superconducting NdFeAsO_{1-x}F_x ($T_C = 43$ K for $x = 0.15$) by high-resolution synchrotron x-ray powder diffraction, magnetization, and ⁷⁵As NMR measurements. Structural investigations showed a contraction of the lattice structure with shorter RE-As bond distances, an increased thickness of the As-Fe₂-As layer and less distorted Fe-As₄ tetrahedra for the NdFeAsO family when compared to the LaFeAsO family. A typical ⁷⁵As quadrupole powder line shape measured for NdFeAsO yielded an enhanced quadrupole frequency with respect to the La analogs. Furthermore, we calculated the electric field gradient using the band-structure code FPLO and obtained good agreement for the undoped compound. The enhanced EFG is due to a more prolate As 4p electron distribution, which is mainly caused by reduced lattice parameters and not the presence of Nd 4f electrons. We also found a scaling of the ⁷⁵As NMR shift with the magnetic susceptibility of localized Nd moments suggesting a weak coupling between the NdO and FeAs layer. The RKKY- interaction between localized Nd 4f moments mediated by itinerant Fe 3d and/or Nd 5d states may originate from such a coupling.

Acknowledgments

J.W.G.B acknowledges the Royal Society of Edinburgh for financial support. The EPSRC-GB is thanked for

provision of the beam time at the ESRF.

-
- * Electronic address: j.w.g.bos@ed.ac.uk
† Electronic address: serena.margadonna@ed.ac.uk
‡ Electronic address: denis.arcon@ijs.si
- ¹ P. Quebe, L. J. Terbüchte, and W. Jeitschko, *J. Alloys Compd.* **302**, 70 (2000).
 - ² Y. Kamihara, T. Watanabe, M. Hirano, and H. Hosono, *J. Am. Chem. Soc.* **130**, 3296 (2008).
 - ³ H. Takahashi, K. Igawa, K. Arii, Y. Kamihara, M. Hirano, and H. Hosono, *Nature (London)* **453**, 376 (2008).
 - ⁴ Z.-A. Ren, G.-C. Che, X.-L. Dong, J. Yang, W. Lu, W. Yi, X.-L. Shen, Z.-C. Li, L.-L. Sun, F. Zhou, and Z.-X. Zhao, *Europhys. Lett.* **83**, 17002. (2008).
 - ⁵ G. F. Chen, Z. Li, D. Wu, G. Li, W. Z. Hu, J. Dong, P. Zheng, J. L. Luo, and N. L. Wang, *Phys. Rev. Lett.* **100**, 247002 (2008).
 - ⁶ Z.-A. Ren, J. Yang, W. Lu, W. Yi, G.-C. Che, X.-L. Dong, L.-L. Sun, and Z.-X. Zhao, *Mater. Res. Innovations* **12**, 105 (2008).
 - ⁷ Z.-A. Ren, J. Yang, W. Lu, W. Yi, X.-L. Shen, Z.-C. Li, G.-C. Che, X.-L. Dong, L.-L. Sun, F. Zhou, and Z.-X. Zhao, *Europhys. Lett.* **82**, 57002 (2008).
 - ⁸ C. de la Cruz, Q. Huang, J. W. Lynn, Jiyang Li, W. Ratcliff II, J. L. Zarestky, H. A. Mook, G. F. Chen, J. L. Luo, N. L. Wang, and P. Dai, *Nature (London)* **453**, 899 (2008).
 - ⁹ P. Cheng, L. Fang, H. Yang, X. Zhu, G. Mu, H. Luo, Z. Wang, and H. Wen, *Sci. China Ser. G* **51**, 719 (2008).
 - ¹⁰ J. W. G. Bos, G. B. S. Penny, J. A. Rodgers, D. A. Sokolov, A. D. Huxley, and J. P. Attfield, *Chem. Commun. (Cambridge)* 3634 (2008).
 - ¹¹ T. Nomura, S. W. Kim, Y. Kamihara, M. Hirano, P. V. Sushko, K. Kato, M. Takata, A. L. Shluger, and H. Hosono, *Supercond. Sci. Technol.* **21**, 125028 (2008).
 - ¹² H.-H. Klauss, H. Luetkens, R. Klingeler, C. Hess, F. J. Litterst, M. Kraken, M. M. Korshunov, I. Eremin, S. L. Drechsler, R. Khasanov, A. Amato, J. Hamann-Borrero, N. Leps, A. Kondrat, G. Behr, J. Werner, and B. Büchner, *Phys. Rev. Lett.* **101**, 077005 (2008).
 - ¹³ F. Ma, Z.-Y. Lu, and T. Xiang, *Phys. Rev. B* **78**, 224517 (2008).
 - ¹⁴ G. Giovannetti, S. Kumar, and J. van den Brink, *Physica B* **403**, 3653 (2008).
 - ¹⁵ K. Ahilan, F. L. Ning, T. Imai, A. S. Sefat, R. Jin, M.A. McGuire, B. C. Sales, and D. Mandrus, *Phys. Rev. B* **78**, 100501(R) (2008).
 - ¹⁶ Y. Nakai, K. Ishida, Y. Kamihara, M. Hirano, and H. Hosono, *J. Phys. Soc. Jpn.* **77**, 073701 (2008).
 - ¹⁷ H.-J. Grafe, D. Paar, G. Lang, N. J. Curro, G. Behr, J. Werner, J. Hamann-Borrero, C. Hess, N. Leps, R. Klingeler, and B. Büchner, *Phys. Rev. Lett.* **101**, 047003 (2008).
 - ¹⁸ A. C. Larson and R. B. Von Dreele, Los Alamos National Laboratory Report (LAUR) Report No. 86 (2000) (unpublished).
 - ¹⁹ B. H. Toby, *J. Appl. Crystallogr.* **34**, 210 (2001).
 - ²⁰ K. Koepf and H. Eschrig, *Phys. Rev. B* **59**, 1743 (1999).
 - ²¹ J. P. Perdew and Y. Wang, *Phys. Rev. B* **45**, 13244 (1992).
 - ²² The temperature during the room-temperature scan was not controlled so it may have varied for a couple of degrees. Taking a typical value for a thermal expansion coefficient we note that the actual accuracy of the lattice parameters may be less than the ones obtained directly from the Rietveld refinement procedure.
 - ²³ M. Fratini, R. Caivano, A. Puri, A. Ricci, Z. Ren, X.-Li Dong, J. Yang, W. Lu, Z.-X. Zhao, L. Barba, G. Arrighetti, M. Polentarutti, and A. Bianconi, *Supercond. Sci. Technol.* **21**, 092002 (2008).
 - ²⁴ H. Mukuda, N. Terasaki, H. Kinouchi, M. Yashima, Y. Kitaoka, S. Suzuki, S. Miyasaka, S. Tajima, K. Miyazawa, P. M. Shirage, H. Kito, H. Eisaki, and A. Iyo, *J. Phys. Soc. Jpn.* **77**, 093704 (2008).
 - ²⁵ P. Pykkö, *Mol. Phys.* **99**, 1617 (2001).
 - ²⁶ C. Krellner, N. Caroca-Canales, A. Jesche, H. Rosner, A. Ormeci and C. Geibel, *Phys. Rev. B* **78**, 100504(R) (2008).
 - ²⁷ I. I. Mazin, M. D. Johannes, L. Boeri, K. Koepf, and D. J. Singh, *Phys. Rev. B* **78**, 085104 (2008).
 - ²⁸ H.-J. Grafe, G. Lang, F. Hammerath, D. Paar, K. Manthey, K. Koch, H. Rosner, N. J. Curro, G. Behr, J. Werner, N. Leps, R. Klingeler, and B. Büchner, *New J. Phys.* (to be published).
 - ²⁹ K. Koch, R. O. Kuzian, K. Koepf, I. V. Kondakova and H. Rosner (to be published).
 - ³⁰ The supercell calculations were performed for the La compound (Ref. 28). Since the EFG is calculated on the As site and the substituted site is oxygen, a very similar behavior is expected for the Nd compound and there is no need for repeating the supercell calculation.
 - ³¹ A. A. Aczel, E. Baggio-Saitovitch, S. L. Budko, P. C. Canfield, J. P. Carlo, G. F. Chen, P. Dai, T. Goko, W. Z. Hu, G. M. Luke, J. L. Luo, N. Ni, D. R. Sanchez-Candela, F. F. Tafti, N. L. Wang, T. J. Williams, W. Yu, and Y. J. Uemura, *Phys. Rev. B* **78**, 214503 (2008).
 - ³² Y. Chen, J. W. Lynn, J. Li, G. Li, G. F. Chen, J. L. Luo, N. L. Wang, Pengcheng Dai, C. dela Cruz, and H. A. Mook, *Phys. Rev. B* **78**, 064515 (2008).
 - ³³ K. Kitagawa, N. Katayama, K. Ohgushi, M. Yoshida, and M. Takigawa, *J. Phys. Soc. Jpn.* **77**, 114709 (2008).
 - ³⁴ K. Haule, J. H. Shim, and G. Kotliar, *Phys. Rev. Lett.* **100**, 226402 (2008).
 - ³⁵ H. Tou, N. Tsugawa, M. Sera, H. Harima, Y. Haga, and Y. Onuki, *J. Phys. Soc. Jpn.* **76**, 024705 (2007).